Available online at www.sciencedirect.com
ScienceDirect
Trans. Nonferrous Met. Soc. China 25(2015) 3700−3707
Transactions of Nonferrous Metals Society of China
www.tnmsc.cn

Comparison between WC−10Co−4Cr and Cr_3C_2−25NiCr coatings sprayed on H13 steel by HVOF

Wen-chao ZHANG[1], Li-bin LIU[1], Meng-ting ZHANG[2,3], Guo-xing HUANG[1], Jia-si LIANG[1], Xian LI[1], Li-gang ZHANG[1]

1. School of Materials Science and Engineering, Central South University, Changsha 410083, China;
2. Guangzhou Research Institute of Nonferrous Metals, Guangzhou 510650, China;
3. SAIC General Motos Wuling (SGMW) Company, Liuzhou 545007, China

Received 25 November 2014; accepted 21 June 2015

Abstract: WC−10Co−4Cr and Cr_3C_2−25NiCr coatings were deposited on H13 steel by high velocity oxy fuel (HVOF) spraying. To enhance the thermal stability of the WC−10Co−4Cr coating, NiCr powders were sprayed between the surface coating and substrate. The microstructures of the surface and cross section, thermal shock and wear resistance of these two coatings were investigated in detail. The carbon diffusion in the two coatings was explained from the view of the thermodynamic. And the adhesive strength of Cr_3C_2−25NiCr coating (64.40 MPa) is almost the same as that of WC−10Co−4Cr coating (61.69 MPa). The friction tests show that the Cr_3C_2−25NiCr coating has higher friction coefficient than the WC−10Co−4Cr coating at both 500 and 600 °C. The wear resistance of the Cr_3C_2−25NiCr coating is better than that of the WC−10Co−4Cr coating.
Key words: HVOF spraying; WC−10Co−4Cr; Cr_3C_2−25NiCr; wear resistance

1 Introduction

Recently, superior coatings with benign adhesive strength, good wear resistance, high hardness and thermal stability have emerged [1−3], and have been widely used for cutting tools and dies in high-speed manufacturing [4,5].

These coatings acting as a thermal barrier and wear barrier can protect the surface of the hot work die steel against high temperature and abrading [6]. To enhance the surface properties of hot work die steel, hexavalent chromium-based conversion coatings (HCCC) have been extensive used [7,8]. However, hexavalent chromium (Cr^{6+} ions) can lead to serious environment pollution and health problem [8]. Additionally, with the increase of thermal cycles, the HCCC coatings always break from the substrate because of the poor adhesive strength and promote hydrogen embrittlement [9]. The emergence of the thermal spraying techniques especially high velocity oxy fuel (HVOF) provides a possible approach to produce new coatings without above problems.

HVOF combines the oxygen, hydrogen and kerosene together and make the combustion process under the control. The flame temperature can be up to 3000 °C. Thus, it can bring the powders at a very high speed (almost the velocity of sound) and spray them to the substrate. The high-speed spraying method, which can avoid powders to contact the external environment, can improve the density of the coating and reduce oxidation [10]. HVOF can enhance the property of abrasive wear resistance [11,12] and adhesive strength [13−15]. Compared with the conventional coating, WANG et al [12] reported that the microstructure of WC−12Co coating deposited by HVOF exhibits denser coating structure and slightly higher microhardness, which results in better wear resistance. The microhardness of the WC−Co coating deposited with the HVOF technique was $HV_{0.1}$ 932 from the research of MYALSKA et al [13]. It has a very impressive prospect in replacing electrolytic hard chromium [16].

There are no studies in literature regarding a comparison between WC−10Co−4Cr and Cr_3C_2−25NiCr spraying on the hot work die H13 steel via HVOF process. The aim of this study is to produce WC−10Co−4Cr and Cr_3C_2−25NiCr coatings with desirable high

Foundation item: Project (51371200) supported by the National Natural Science Foundation of China; Project (2014CB644000) supported by the National Basic Research Program of China; Project (502044009) supported by the Fundamental Research Funds for the Central Universities, China
Corresponding author: Li-gang ZHANG; Tel: +86-731-88877732; E-mail: Ligangzhang@csu.edu.cn
DOI: 10.1016/S1003-6326(15)64011-0

temperature tribology properties by HVOF. Additionally, because the thermal stability of WC is weaker than that of Cr_3C_2 according to the simulation results of the TC software, NiCr was used to spray between the WC−10Co−4Cr and the substrate to suppress decarburization in this study.

2 Experimental

The H13 steel was selected as substrate. The sample dimensions are 100 mm × 100 mm × 80 mm. Before spraying, the surface was washed by acetone. After degreasing, the surface was pretreated with sand-blasting to improve the adhesion between the coating and the substrate. The chemical composition of the H13 steel used in this work is listed in Table 1.

Table 1 Chemical composition of H13 steel (mass fraction, %)

Fe	C	Mn	Si	Cr
89.60−92.00	0.32−0.45	0.20−0.50	0.80−1.20	4.75−5.50
P	S	Mo	V	
≤0.03	≤0.03	1.10−1.75	0.80−1.20	

In the spraying process, the flame temperature, flame speed and flight distance are very important factors affecting the state of melting and the formation of the coating [17,18]. The HVOF spraying parameters used in this work are given in Table 2.

Representative SEM micrographs of the three powders are shown in Fig. 1. The figures show that the sizes of the powders WC−10Co−4Cr, Cr_3C_2−25NiCr and NiCr are around 5−35 μm, 5−40 μm and 10−50 μm, respectively.

The surface treated specimens were cut, ground with SiC abrasive paper, and finally polished with 1 μm diamond abrasive paper. The microstructure of each sample was examined using scanning electron microscopy (SEM) (FEI-Quanta 200). X-ray diffraction with 2θ scanning range of 10° to 80° using Cu K_α radiation was used to characterize whether the decarburization happened in the coating. The Jade 6.0 software with powder diffraction file (PDF 2009) was used for phase analysis.

Two samples with the size of *d*25.4 mm have been cemented with E7 glue. The glued samples have been kept at 100 °C for 3 h to solidify. The adhesive strength was measured by means of tensile testing, employing a JDL−50KN equipment, adopted by ASTM−633 standard. To prevent the shear forces, the two samples must be kept coaxial. Each coating was tested three times to achieve the mean value.

The thermal stability of each phases was calculated with Thermal-Calc developed by SUNDMAN et al [19] using SSUB (TC Substance) database. Temperature of T=773 K, pressure p=1×10^5 Pa, n=1 mol, compositions (x(W)=50% for WC phase, x(W)=33% for W_2C phase, x(Cr)=40% for Cr_3C_2 phase, x(Cr)=30% for Cr_7C_3 phase, x(Cr)=21% for $Cr_{23}C_6$ phase) were set to be the initial conditions of calculation.

For high thermal conductivity materials, when a piece of material is cooled quickly, a temperature gradient is produced. This gradient can lead to different amounts of contraction in different areas. If residual

Table 2 Parameters for high velocity oxy fuel process

Powder	Kerosene flow rate/(L·h^{-1})	Oxygen flow rate/(L·h^{-1})	Oxygen/ oil ratio	Nitrogen flow rate/(L·min^{-1})	Speed of plate/(r·min^{-1})	Thickness/ μm	Spray distance/mm
Cr_3C_2−25NiCr	26.0	900	1.01	12 (L) 11 (R)	3.0	320	380
NiCr	26.0	900	1.01	13 (L) 12 (R)	1.5	100	350
WC−10Co−4Cr	26.0	900	1.02	13 (L) 11 (R)	2.0	320	380

Fig. 1 SEM photographs of three powders: (a) WC−10Co−4Cr; (b) Cr_3C_2−25NiCr; (c) NiCr

tensile stresses become high enough, flaws may propagate and lead to failure. Similar behavior can occur if a material is heated rapidly. This failure of a material caused by stresses induced by sudden changes in temperature is known as thermal shock [20]. The thermal shock performance was performed by thermal fatigue testing machine developed by Jilin University in China. The sizes of the samples were 100 mm × 100 mm × 80 mm, and four edges were ground into chamfering to reduce stress concentration. The parameters of the test are listed in Table 3.

Table 3 Parameters of thermal shock test

Heat temperature/°C	Heating delay/min	Water quenched delay/s	Thermal shock times
600	5	30	15, 30

Friction tests were employed by UMT−3 ball-on-disc wear and friction equipment. The samples were sectioned to *d*25.4 mm × 6 mm and polished to make the surface roughness as R_a<0.35 μm. The parameters of wear tests are listed in Table 4.

In this experiment, the friction coefficient could be obtained directly from the apparatus. However, the wear rates of the coatings need to be used in the interference

Table 4 Parameters of wear test

Environment	Friction pair	Rotational speed/(m·s^{-1})	Load/ N	Temperature/ °C	Time/ min
Nitrogen dry friction	Si_3N_4 friction ball	0.2	11	500 600	20

profiler BMT-Expert 3D to achieve the wear depth and width data. Meanwhile, the data were used to calculate the integral area (V_w, mm^3). Thus, the wear rate (Q) could be calculated by Eq. (1) [21].

$$Q = \frac{V_w}{NS} \tag{1}$$

where S is the total sliding distance (m), and N is the load (N).

3 Results and discussion

3.1 Microstructural investigations

The microstructures of WC−10Co−4Cr/NiCr and Cr_3C_2−25NiCr coated on H13 steel are shown in Fig. 2. It is obvious that WC, Cr_3C_2, NiCr particles are distributed homogeneously on the surface. The two kinds of the coatings all show uniform structure, while

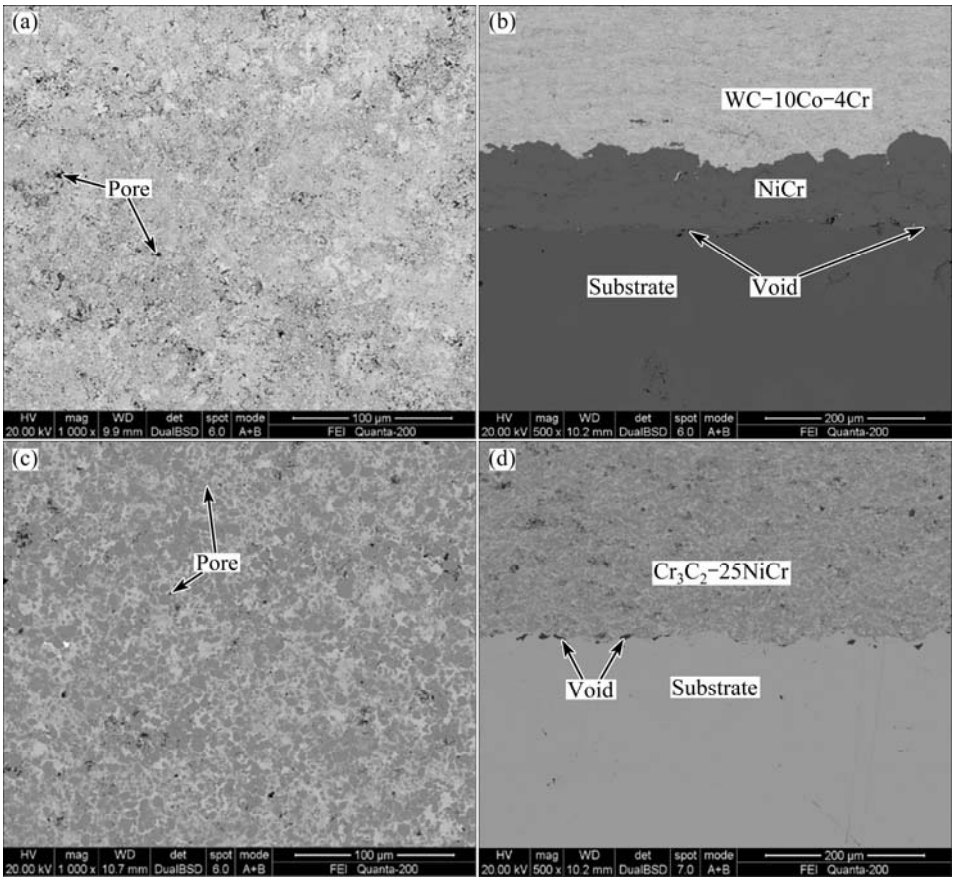

Fig. 2 SEM photographs of WC−10Co−4Cr and Cr_3C_2−25NiCr coated on H13 steel: (a) WC−10Co−4Cr (plan view); (b) WC−10Co−4Cr (cross-section); (c) Cr_3C_2−25NiCr (plan view); (d) Cr_3C_2−25NiCr (cross-section)

WC−10Co−4Cr exhibits a more dense structure (Figs. 2(b) and (d)). In the spraying process, the small particles were completely melted, then cooled rapidly when deposited on the substrate. Some pores are observed on the top of the coatings (Figs. 2(a) and (c)). It can be found from Fig. 2(b) that no obvious cracks can be seen in the WC−10Co−4Cr surface layer and the NiCr transition layer, while some voids indicated by arrows can be found at the interface between the NiCr transition layer and substrate. For Cr_3C_2−25NiCr surface layer, some voids also can be seen at the interface (Fig. 2(d)).

3.2 XRD investigation

The phases in WC−10Co−4Cr and Cr_3C_2−25NiCr powders and coatings have been investigated by X-ray diffraction (XRD). The XRD results are shown in Fig. 3. It is obvious that W_2C phase formed in the WC−10Co−4Cr coating, and Cr_7C_3, $Cr_{23}C_6$ phases formed in the Cr_3C_2−25NiCr coating. BOLELLI et al [22] also reported that W_2C phase formed during the HVOF-spraying process. The formation of these phases could be attributed to the decarburization during the spraying process.

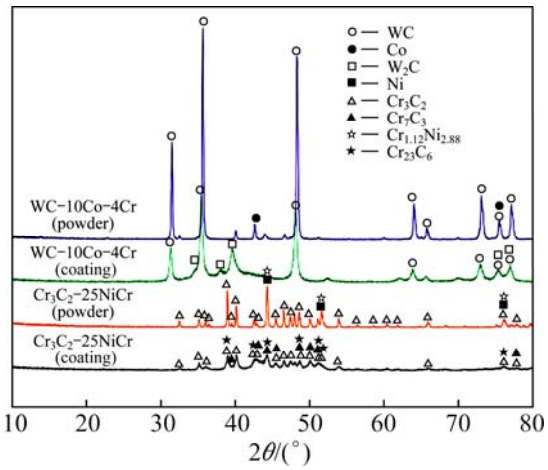

Fig. 3 XRD patterns of WC−10Co−4Cr and Cr_3C_2−25Ni powders and coatings

3.3 Thermal stability

The calculated Gibbs free energies by Thermal-Calc software [23,24] of each phase in the two coatings are shown in Fig. 4. It can be easily found that the thermal stability of WC phase is lower than that of W_2C phase from 2000 K to 3000 K, and above 2500 K, the order of the relative stability of chromium carbides is $Cr_{23}C_6$> Cr_7C_3>Cr_3C_2. During the HVOF process, the temperature is up to 3000 °C. Based on the calculated result, W_2C, $Cr_{23}C_6$ and Cr_7C_3 phases are more stable than WC and Cr_3C_2 and can form during the HVOF process. These calculated results are in good agreement with the XRD results.

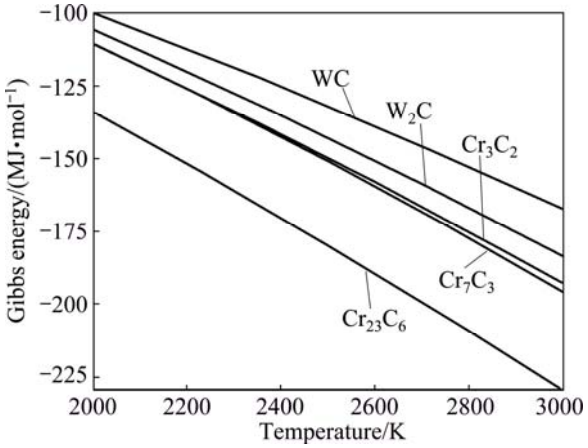

Fig. 4 Calculated Gibbs free energies of phases in WC−10Co−4Cr and Cr_3C_2−25Ni coatings

3.4 Adhesive strength

The adhesive strengths of WC−10Co−4Cr and Cr_3C_2−25NiCr coatings are shown in Table 5. It can be seen that the adhesive strengths of Cr_3C_2−25NiCr and WC−10Co−4Cr coating are almost the same. LI et al [25] reported that the adhesive strength of WC cermet coatings is approximately 65 MPa and Cr_3C_2−25NiCr ranged from 35 MPa to over 90 MPa influenced by spray parameters, which fits well with the results (61.69 MPa in WC−10Co−4Cr and 64.40 MPa in Cr_3C_2−25NiCr) in this study.

Table 5 Adhesive strength of two coatings

Coating	σ/MPa			
	1	2	3	Mean value
WC−10Co−4Cr	55.02	68.17	61.89	61.69
Cr_3C_2−25NiCr	70.77	65.15	57.27	64.40

3.5 Thermal shock performance

Figure 5 shows the typical SEM photographs of the WC−10Co−4Cr and Cr_3C_2−25NiCr coatings after thermal shock testing. A complete crack can be seen, which initiated on the surface of the WC−10Co−4Cr coating after thermal shock 15 times. Due to the effect of stress concentration, cracks propagated forward to release stress. Meanwhile, many crack branches can be found in Fig. 5. The main cracks can develop in the direction of depth until the stress is released completely. JAFARI et al [26] reported the similar occurrence of cracks on the surface of WC−12Co and WC−17Co coatings. For Cr_3C_2−25NiCr coating, a diffusion layer can be seen between the surface coating and the substrate after 30 times of thermal shocking. The thickness of the diffusion layer is 3−11 μm. Due to the increasing times of the thermal shock, C, Cr, Ni and O atoms diffuse into the matrix, which leads to the formation of the diffusion

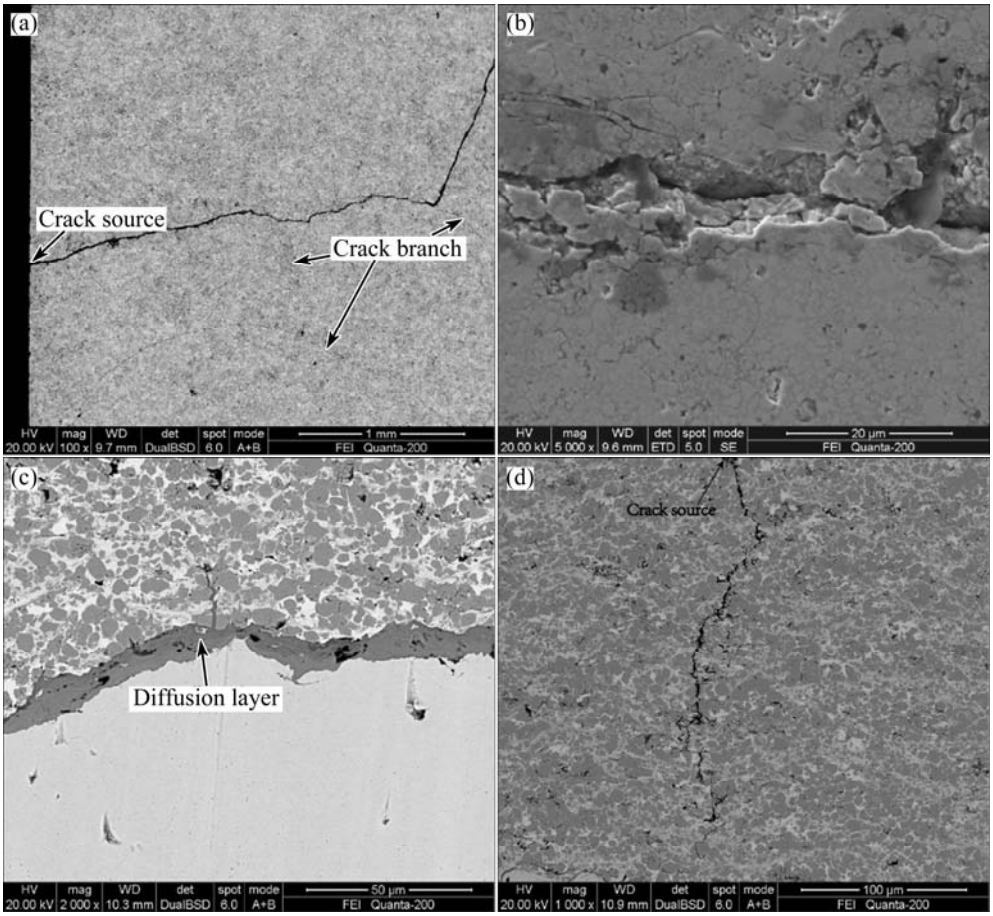

Fig. 5 BSE image (a) and ETD image (b) of WC−10Co−4Cr coating after shocking 15 times, BSE image of Cr_3C_2−25NiCr coating after shocking 30 times (c) and 60 times (d) (cross-sectional view)

layer as shown in Fig. 5(c). After 60 times of thermal shock, a longitudinal crack can be observed in the coating and it also initiated on the surface of the coating (Fig. 5(d)).

3.6 Friction and wear behavior

The friction coefficients of WC−10Co−4Cr and Cr_3C_2−25NiCr coatings tested at 500 and 600 °C are shown in Fig. 6, which indicates that the wear process included a temporary running-in stage at the beginning of the wear tests, a stage showing slow increase in friction coefficient and the final steady-state for the WC−10Co−4Cr coating. While for the Cr_3C_2−25NiCr coating, a significant drop in friction coefficient at 600 °C can be found after 200 s due to the crack formation during the wear test. The mean values of friction coefficient, after reaching the steady-state, are listed in Table 6.

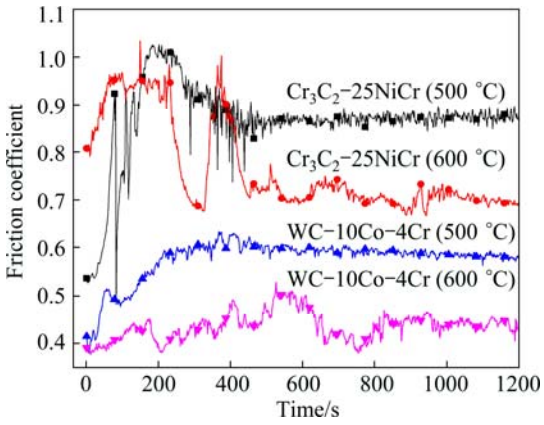

Fig. 6 Friction curve of coatings

Table 6 Steady-state friction coefficients of coatings at different temperatures

Coating	500 °C	600 °C
WC−10Co−4Cr	0.59	0.44
Cr_3C_2−25NiCr	0.87	0.70

3.7 Wear track profiles

The cross-sectional profiles of wear tracks on the two coatings after wear tests are shown in Fig. 7. It can be seen that the wear tracks on the WC−10Co−4Cr coating are obvious, but those on the Cr_3C_2−25NiCr coating are too shallow to be measured, which indicates that the wear resistance of the Cr_3C_2−25NiCr coating is better than that of the WC−10Co−4Cr coating.

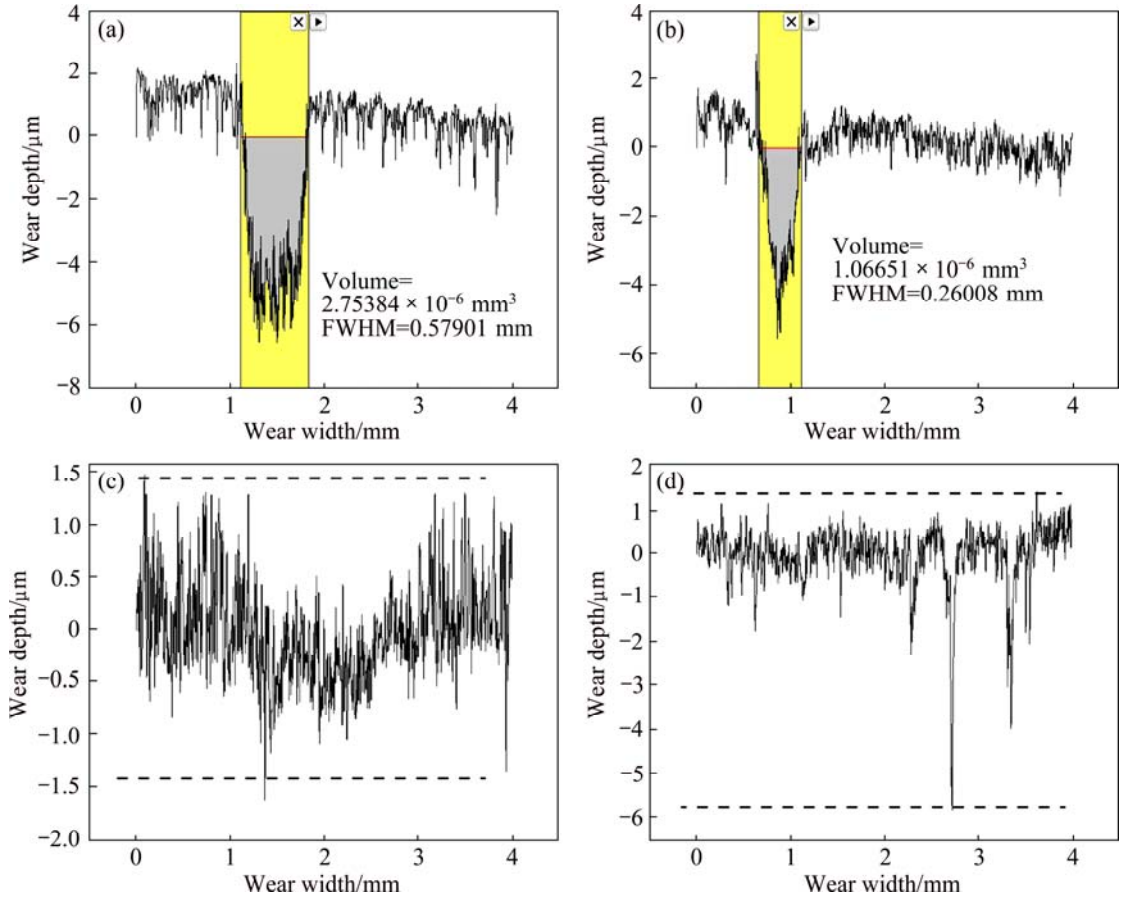

Fig. 7 Cross-sectional profiles of wear tracks on WC−10Co−4Cr coating tested at 500 °C (a) and 600 °C (b) and Cr_3C_2−25NiCr coating tested at 500 °C (c) and 600 °C (d)

The wear tracks on each sample were measured for four times to get the average value of wear volume which is listed in Table 7. Based on Eq. (1), the wear rates of WC−10Co−4Cr are calculated to be 9.5819×10^{-8} $mm^3/(N\cdot m)$ at 500 °C and 4.2659×10^{-8} $mm^3/(N\cdot m)$ at 600 °C. The results are in the same magnitude of those reported by SHIPWAY et al [27] and ZHAO et al [28], which are 10.5×10^{-8} $mm^3/(N\cdot m)$ under the condition of 19 N load using alumina balls (*d*9.6 mm) and 4×10^{-8} $mm^3/(N\cdot m)$ under the condition of 5 N load using Si_3N_4 balls (*d*3 mm), respectively.

Table 7 FWHM and wear track volumes in WC−10Co−4Cr coating

Test No.	500 °C		600 °C	
	Wear volume/ (10^{-6} mm^3)	FWHM/ mm	Wear volume/ (10^{-6} mm^3)	FWHM/ mm
1	2.75384	0.57901	1.06651	0.26008
2	2.43486	0.59074	1.00553	0.21313
3	2.48706	0.50944	1.39902	0.26171
4	2.44274	0.53756	1.03375	0.23203
Mean	2.52963	0.55419	1.12620	0.24174

4 Conclusions

1) These two kinds of coatings all show uniform structure, while WC−10Co−4Cr exhibits a more dense structure. The W_2C phase forms in the WC−10Co−4Cr coating and Cr_7C_3, $Cr_{23}C_6$ phases form in the Cr_3C_2−25NiCr coating mainly due to the decarburization during spraying, and these results quite agree with the calculated thermal stability of each phase using the Thermal-Calc software.

2) The thermal shock experiments show that a complete crack initiates on the surface of the WC−10Co−4Cr coating after thermal shock for 15 times and the coating starts to peel and expire. The cracks have not been found in the Cr_3C_2−25NiCr coating after thermal shock for 15 and 30 times. After thermal shock 60 times, the micro crack has been found at the interface of the coating.

3) The friction tests show that the friction coefficient of the two coatings at 500 °C is higher than that at 600 °C. The Cr_3C_2−25NiCr coating exhibits higher friction coefficient than the WC−10Co−4Cr

coating at both 500 °C and 600 °C. By the comparison of the wear tests, the Cr_3C_2−25NiCr coating shows better wear resistance and higher friction coefficient than the WC−10Co−4Cr coating at both 500 °C and 600 °C.

References

[1] BROSZEIT E, MATTHES B, HEN W, KLOOS K. Tribological properties of fry sputtered Ti−BN coatings under various pin-on-disc wear test conditions [J]. Surface and Coatings Technology, 1993, 58(1): 29−35.

[2] SHOBU K, WATABABE T, DRENNAN J, HANNINK R H J, SWAIN M V. Toughening mechanisms and microstructures of TiB_2–ZrO_2 composites [J]. Advanced Materials, 1986, 24: 1091−1099.

[3] HAN M S, LEE S J, KIM M S, JANG S K, KIM S J. Electrochemical characteristics of HVOF spray coated layer with WC−27NiCr and WC−10Co4Cr for Al bronze [J]. Transactions of Nonferrous Metals Society of China, 2012, 22(S): s753−s759.

[4] AZADI M, ROUHAGHDAM A S, AHANGARANI S, MOFIDI H. Mechanical behavior of TiN/TiC multilayer coatings fabricated by plasma assisted chemical vapor deposition on AISI H13 hot work tool steel [J]. Surface and Coatings Technology, 2014. 245: 156−166.

[5] FREYMAN C A, CHUNG Y W. Synthesis and characterization of hardness-enhanced multilayer oxide films for high-temperature applications [J]. Surface and Coatings Technology, 2008, 202(19): 4702−4708.

[6] BOLELLI G, LUSVARGHI L, BARLETTA M. Heat treatment effects on the corrosion resistance of some HVOF-sprayed metal alloy coatings [J]. Surface and Coatings Technology, 2008, 202(19): 4839−4847.

[7] NATISHAN P, LAWRENCE S, FOSTER R, LEWIS J, SARTWELL B. Salt fog corrosion behavior of high-velocity oxygen-fuel thermal spray coatings compared to electrodeposited hard chromium [J]. Surface and Coatings Technology, 2000, 130(2): 218−223.

[8] SERRES N, HLAWKA F, COSTIL S, LANGLADE C, MACHI F, CONET A. Dry coatings and ecodesign, part 1—Environmental performances and chemical properties [J]. Surface and Coatings Technology, 2009, 204(1): 187−196.

[9] SARTWELL B D, LEGG K O, SCHELL J, SAUER J, NATISHAN P. Validation of HVOF WC/Co thermal spray coatings as a replacement for hard chrome plating on aircraft landing gear [R]. Washington D C: Naval Research Lab, 2004.

[10] MA Jing, YAN Dong-qing, HU Jian-wen, ZHANG Xin, LI Yang. Reactive HVOF sprayed TiN-matrix composite coating and its corrosion and wear resistance properties [J]. Transactions of Nonferrous Metals Society of China, 2013, 23(4): 1011−1018.

[11] WANG Shan-lin, CHENG Jing-chang, YI Seong-hoon, KE Li-ming. Corrision resistance of Fe-based amorphous metallic matrix coating fabricated by HVOF thermal spraying [J]. Transactions of Nonferrous Metals Society of China, 2014, 24(1): 146−151.

[12] WANG Q, CHEN Z, DING Z. Performance of abrasive wear of WC−12Co coatings sprayed by HVOF [J]. Tribology International, 2009, 42(7): 1046−1051.

[13] MYALSKA H, MOSKAL G, SZYMANSKI K. Microstructure and properties of WC−Co coatings, modified by sub-microcrystalline carbides, obtained by different methods of high velocity spray processes [J]. Surface and Coatings Technology, 2014, 206: 303−309.

[14] MASOUMI H, SAFAVI S M, SALEHI M, NAHVI S M. Effect of grinding on the residual stress and adhesion strength of HVOF thermally sprayed WC−10Co−4Cr coating [J]. Materials and Manufacturing Processes, 2014, 29(9): 1139−1151.

[15] BOLELLI G, BERGER L M, BONETTI M, LUSVARGHI L. Comparative study of the dry sliding wear behaviour of HVOF-sprayed WC–(W,Cr)2C−Ni and WC−CoCr hardmetal coatings [J]. Wear, 2014, 309(1): 96−111.

[16] PUCHICABRERA E, LESAGE M S, GIL L, VILLALOBOSGUTIERREZ C. Fatigue behavior of AA7075-T6 aluminum alloy coated with ZrN by PVD [J]. International Journal of Fatigue, 2008, 30(7): 1220−1230.

[17] WANG Q, CHEN Z, LI L, YANG G. The parameters optimization and abrasion wear mechanism of liquid fuel HVOF sprayed bimodal WC−12Co coating [J]. Surface and Coatings Technology, 2012, 206(8): 2233−2241.

[18] HONG S, WU Y, WANG B, ZHENG Y, GAO W, LI G. High-velocity oxygen-fuel spray parameter optimization of nanostructured WC−10Co−4Cr coatings and sliding wear behavior of the optimized coating [J]. Materials and Design, 2014, 55: 286−291.

[19] SUNDMAN B, JANSSON B, ANDERSSON J O. The thermo-calc databank system [J]. CALPHAD, 1985, 9(2): 153−190.

[20] ASKELAND D, FULAY P, WRIGHT W. The science and engineering of materials [M]. Cengage Learning, 2011.

[21] HUANG Y, FAN H, WANG D, SUN Y, LIU F, SHEN J, SUN J, MI J. The effect of cooling rate on the wear performance of a ZrCuAlAg bulk metallic glass [J]. Materials and Design, 2014, 58: 284−289.

[22] BOLELLI G, BORNER T, MILANTI A, LUSVARGHI L, LAURILA J, KOIVULUOTO H, NIEMI K, VUORISTO P. Tribological behavior of HVOF-and HVAF-sprayed composite coatings based on Fe-alloy+WC−12%Co [J]. Surface and Coatings Technology, 2014, 248: 104−112.

[23] ZHANG L G, MASSET P J, TAO X M, HUANG G X, LUO H T, LIU L B, JIN Z P. Thermodynamic description of the Al−Cu−Y ternary system [J]. CALPHAD, 2011, 35: 574−579.

[24] WANG X, LIU L B, WANG M F, SHI X, HUANG G X, ZHANG L G. Computational modeling of elastic constants as a function of temperature and composition in Zr−Nb alloys [J]. CALPHAD, 2015, 48: 89−94.

[25] LI C J, WANG Y Y, WU T, JI G C, OHMORI A. Effect of types of ceramic materials in aggregated powder on the adhesive strength of high velocity oxy-fuel sprayed cermet coatings [J]. Surface and Coatings Technology, 2001, 145(1): 113−120.

[26] JAFARI M, ENAYTI M, SALEHI M, NAHVI S, PARK C. Improvement in tribological properties of HVOF sprayed WC−Co coatings using electroless Ni–P coated feedstock powders [J] Surface and Coatings Technology, 2013, 235: 310−317.

[27] SHIPWAY P, MCCARTNEY D, SUDAPRASERT T. Sliding wear behaviour of conventional and nanostructured HVOF sprayed WC−Co coatings [J]. Wear, 2005, 259(7): 820−827.

[28] ZHAO X Q, ZHOU H D, CHEN J M. Comparative study of the friction and wear behavior of plasma sprayed conventional and nanostructured WC−12% Co coatings on stainless steel [J]. Materials Science and Engineering A, 2006, 431(1): 290−297.

在 H13 钢上超音速火焰喷涂制备 WC−10Co−4Cr 和 Cr_3C_2−25NiCr 涂层的性能比较

张文超[1]，刘立斌[1]，张梦婷[2,3]，黄国幸[1]，梁佳思[1]，李 显[1]，章立钢[1]

1. 中南大学 材料科学与工程学院，长沙 410083；
2. 广州有色金属研究院，广州 510650;
3. 上汽通用五菱汽车股份有限公司，柳州 545007

摘 要：在 H13 钢基体上采用超音速火焰喷涂方式制备一定厚度的 WC−10Co−4Cr 和 Cr_3C_2−25NiCr 涂层。为了增加 WC−10Co−4Cr 涂层的热稳定性，在涂层和基体之间加喷了 NiCr 喷涂粉末。研究了这两种硬质合金涂层的表面及横截面的微观形貌、抗热震性和耐磨损性能。从热力学的角度解释了两种涂层中出现的碳扩散现象。Cr_3C_2−25NiCr 涂层的结合强度(64.40 MPa) 和 WC−10Co−4Cr 涂层的结合强度(61.69 MPa)基本相同。通过摩擦磨损试验研究发现，两种涂层在 600 °C 的摩擦因数均比在 500 °C 时的小，Cr_3C_2−25NiCr 的耐磨损性能比 WC−10Co−4Cr 的要好。

关键词：超音速火焰喷涂；WC−10Co−4Cr；Cr_3C_2−25NiCr；摩擦磨损性能

(Edited by Yun-bin HE)